Analytical Biochemistry 567 (2019) 51–62

Contents lists available at ScienceDirect

Analytical Biochemistry

journal homepage: www.elsevier.com/locate/yabio

A novel catalase mimicking nanocomposite of Mn(II)-poly-L-histidine-carboxylated multi walled carbon nanotubes and the application to hydrogen peroxide sensing

Jiexin Zhou[a,1], Yuan Chen[a,1], Lintao Lan[a], Cong Zhang[b,**], Meixin Pan[a], Yingying Wang[a], Bingkai Han[a], Zihua Wang[a], Jun Jiao[a], Qiang Chen[a,*]

[a] The Key Laboratory of Bioactive Materials Ministry of Education, College of Life Science, Nankai University, Weijin Road No.94, Tianjin, 300071, China
[b] Department of Chemistry, School of Sciences, Hebei University of Science and Technology, Shijiazhuang, 050018, China

ARTICLE INFO

Keywords:
Mn(II)
Poly-L-histidine
Multi walled carbon nanotubes
Hydrogen peroxide
Biosensor

ABSTRACT

In this work, a novel enzyme-mimicking nanocomposite of Mn(II)-poly-L-histidine (PLH) functionalized carboxylated multi walled carbon nanotubes (CMWCNTs) was designed and synthesized. Based on the catalase-like activity of the nanocomposite, a non-enzymatic hydrogen peroxide (H_2O_2) biosensor was then established and explored for H_2O_2 electrochemical detection. The nanocomposite was characterized by Fourier transform infrared spectra, Raman spectroscopy, and transmission electron microscopy. Due to the enlarged effective surface area and the efficient electrocatalytic activity of the Mn(II)-PLH redox-active units, the obtained Mn(II)-PLH-CMWCNT electrode showed excellent electrocatalytic performance toward H_2O_2 disproportionation. Under the selected optimum conditions, the prepared biosensor exhibited highly sensitive response toward H_2O_2, and the response current had a good linear relationship between the response currents and H_2O_2 concentrations in the range of 0.002–1.0 mM, a low detection limit of 0.5 μM and a sensitivity of 464.18 μA mM^{-1} cm^{-2}. With the good stability, reproducibility and selectivity, the proposed biosensor was successfully applied to the determination of H_2O_2 in real-life samples, and showed satisfactory results. In summary, the Mn(II)-PLH-CMWCNT nanocomposite could be a promising enzyme-mimicking nanomaterial for the researches of electrocatalysis, biosensing and relevant fields.

1. Introduction

Hydrogen peroxide (H_2O_2), commonly generated as a by-product of several oxidase catalysis reactions, plays an important role as a signal molecule in regulating diverse biological processes including cell division, apoptosis, cellular immune response, vascular reconstruction, stomatal closure and root growth [1]. Meanwhile, in addition to the above functions, hydrogen peroxide has also been considered to serve pivotal roles in causing oxidative damage, as an infaust but inevitable consequence of aerobic metabolism [2–4]. On the other hand, hydrogen peroxide is also an important indicator in food and drug supervision, environmental monitoring, and clinical diagnosis. Therefore, a rapid and sensitive method for hydrogen peroxide detection is of great importance both in the academic and industrial fields. Up to now, various techniques for hydrogen peroxide determination have been developed such as high performance liquid chromatography (HPLC) [5], electrochemistry [6], chemiluminescence [7], fluorescence [8] and spectrophotometry [9]. Among them, electrochemical methods have attracted significant attention due to the low cost, simple operation, rapid response, high sensitivity and selectivity [10]. Parnell et al. reported a non-enzymatic hydrogen peroxide sensor using a cobalt(III) complex supported on carbonaceous nanomaterials, which showed excellent electrocatalytic activity for H_2O_2 reduction [11]. In recent years, carbonaceous nanomaterials strategies based on transition metal coordination polymers are attracting great interest.

Multi walled carbon nanotubes (MWCNTs) have received much attention. since Japanese scientist Iijima discovered the coaxial nanotubular nanomaterials [12]. Based on the excellent mechanical and electronic properties of nanostructures, MWCNTs are widely used in the fields of biosensors [13], catalysis [14], drug delivery [15], energy

* Corresponding author.
** Corresponding author.
E-mail addresses: zhangcong0672@163.com (C. Zhang), qiangchen@nankai.edu.cn (Q. Chen).
[1] These authors contributed equally, as co-first authors, to this study.

https://doi.org/10.1016/j.ab.2018.12.007
Received 26 July 2018; Received in revised form 5 December 2018; Accepted 9 December 2018
Available online 11 December 2018
0003-2697/

storage [16], *etc*. An efficient multipurpose method of chemical oxidation treatment with mixed acid is used to improve MWCNTs, which could not only improve the dispersion capability of MWCNTs, but also enhance the chemical activity by introducing carboxylic acid (-COOH) functional groups, which can be further easily modified [17].

In the current work, poly-L-histidine (PLH), as an excellent polyelectrolyte, was innovatively introduced to modify carboxylated multi walled carbon nanotubes (CMWCNTs). Because of the lipophilic π-π conjugated aromatic structures of imidazole groups on the side chain, PLH will non-covalently interact with the exterior walls of CMWCNTs. In addition, the free amino groups of PLH will also covalently interact with carboxyl groups of CMWCNTs by forming amide bonds. The π-π interactions play important roles in the electron transfer process, thus the combination of PLH and carbon nanotubes could increase electron transfer dramatically [18,19]. Moreover, after the imidazole group of PLH was combined with metal ions, the transfer of charge to the nanotubes would be greatly enhanced. Specifically, it was found that the ions (atoms)-PLH composites possess obvious catalytic activities for many reactions [20,21].

Growing evidences suggest that Mn(II) ions play important roles in protecting cells and tissues from oxygen radical damage [22]. For example, mitochondrial superoxide dismutase is a Mn(II) containing enzyme [23]. Additionally, iron loaded enzymes are vulnerable to the Fenton reagent, but importing manganese may prevent protein damage [24]. Recent studies indicate that many manganese-based compounds or manganese complexes have peroxidase or catalase-like activities, and are widely used in the fields of biocatalysts and biosensors. More evidences have supported the concept that manganese complexes could be efficient peroxidase or catalase mimics. Natarajan et al. reported a biomimicking functional model system based on $[MnII(bpy)_2(H_2O)_2]^{2+}$ complex. The results highlight the electrocatalytic activity towards the H_2O_2 oxidation and reduction reactions as like the Mn-pseudocatalase enzyme system (Mn-CAT) [25]. In addition, by combining with different ligands, manganese complexes might exert many different features and functions.

To the best of our knowledge, the strategy involving a Mn(II)-PLH functionalized CMWCNT (Mn(II)-PLH-CMWCNT) composite for the determination of H_2O_2 has not ever been reported. In this study, a non-enzymatic biosensor was successfully fabricated by drop-coating the Mn (II)-PLH-CMWCNT nanocomposite on a glassy carbon electrode (GCE) before it was applied to H_2O_2 detection. Additionally, with the excellent electrocatalytic activity, stability, reproducibility, and selectivity, the developed biosensor will provide the potential in real-life samples determination.

2. Materials and methods

2.1. Chemicals and reagents

PLH (molecular weight 5000-25,000 Da), H_2O_2 solution (30 wt% in H_2O), manganese(II) chloride tetrahydrate, sodium bicarbonate, D-glucose, uric acid, L-ascorbic acid, acetaminophen, N-(3-dimethylaminopropyl)-N′-ethylcarbodiimide hydrochloride (EDC) and N-hydroxysuccinimide (NHS) were purchased from Sigma–Aldrich. MWCNTs (20–50 nm diameter, 10 μm average length and 95% purity) were purchased from Institute of Organic Chemistry, Chinese Academy of Sciences (Chengdu, China). H_2SO_4 (98%), HNO_3 (65%), KCl, $K_3Fe[(CN)_6]$, Na_2HPO_4 and NaH_2PO_4 were purchased from Tianjin Damao Chemical Reagent Factory (Tianjin, China). All the chemicals and reagents were of analytical reagent grade and used as received without further purification. Deionized water was used throughout the experiments unless otherwise indicated.

2.2. Preparation of the Mn(II)-PLH-CMWCNT/GCE

CMWCNTs were prepared by the chemical oxidation treatment with mixed acid [26]. Initially, 5 mg MWCNTs were ultrasonically dispersed in a mixture containing 11.25 mL of H_2SO_4 and 3.75 mL HNO_3 at 60 °C for 4 h. The reaction product was then centrifuged and washed with deionized water several times until the pH was nearly neutral. In this way, CMWCNTs were obtained after vacuum drying.

Initially, a GCE was sequentially polished using 0.3, 0.1 and 0.05 μm alumina powder. The electrode was next treated in a piranha solution (30% H_2O_2/98% H_2SO_4, 1/3, v/v) at 90 °C for 10 min, followed by alternate ultrasonic cleaning in deionized water and absolute ethanol (3 times, 2 min each time), and then dried with high purity nitrogen. (Warning: piranha solutions are dangerous. Work should be performed in a well ventilated fume hood, small amounts should be employed, and appropriate disposal procedures should be followed.)

The functionalization of CMWCNTs with Mn(II)-PLH was carried out by the following procedure: 2 mM (final concentration, similarly hereinafter) EDC and 5 mM NHS were added into 1 mg/mL CMWCNTs dispersed in 0.1 M phosphate buffered saline (PBS; pH 5.8) and reacted for 15 min at room temperature, followed by adding 20 mM 2-mercaptoethanol to quench EDC and NHS. Then CMWCNTs were centrifuged and redissolved in 0.1 M PBS (pH 5.8) to remove the excess agents. The modification of PLH was carried out by adding 1 mg/mL PLH (dissolved in 0.1 M HCl) to react for another 2 h. Finally, 0.1 M $MnCl_2$ was added to react for another 2 h. Then, a Mn(II)-PLH-CMWCNT composite was obtained by centrifugation and redissolution in deionized water, and quantified to equivalent 1 mg/mL CMWCNTs.

Subsequently, a non-enzymatic hydrogen peroxide biosensor was developed by drop-coating 10 μL of the above nanocomposite onto the surface of a freshly cleaned GCE (denoted as a Mn(II)-PLH-CMWCNT/GCE), which was then dried and stored at room temperature before use. The fabrication process is shown in Scheme 1 below.

2.3. Measurements

Transmission electron microscope (FEI, Tecnai G2 F20), equipped with a high angle energy dispersive X-ray detector, was applied to characterize the prepared nanomaterials. Fourier-transform infrared spectroscopy (FTIR) was conducted on a Bruker TENSOR37 (German) spectrometer with KBr pressed pellet transmission mode. Raman spectra were obtained with a Bruker RFS 100/S (German) spectrometer.

Electrochemical determination of H_2O_2 was conducted using cyclic voltammetry (CV) and chronoamperometry (CA). All electrochemical experiments were carried out using a potentiostat-galvanostat electrochemical workstation (EG&GPARC Model 283, with M270 software) with a conventional three-electrode system. A modified or an unmodified GCE (3 mm diameter) was used as the working electrode; in conjunction with an Ag/AgCl (saturated with KCl) reference electrode and a Pt wire (1 mm diameter) counter electrode. All electrochemical experiments were performed at room temperature.

3. Results and discussion

3.1. Characterization of the Mn(II)-PLH-CMWCNT nanocomposite

We have carried out several control experiments and physicochemical characterizations to identify the true structure of the Mn complex. Details are given below. Raman spectroscopy is a powerful tool to study the defect structures and doping levels of the MWCNT composite. As can be seen in Fig. 1A, a D band (around 1300 cm^{-1}) originates from the sp^2 carbons of in-plane substitutional heteroatoms, vacancies and other defects, while a G band (around 1600 cm^{-1}) is assigned to the graphitic in-plane tangential stretching mode, the intensity ratio (based on the area under the peaks) of the D to G band (I_D/I_G) indicates the degree of defect and doping level of the MWCNTs composites [27–29]. The I_D/I_G value was observed to increase from 1.00 (MWCNTs) to 1.04 (CMWCNTs), suggesting an increase of defect sites resulted from the mixed acid treatment. On the other hand, the $I_D/$

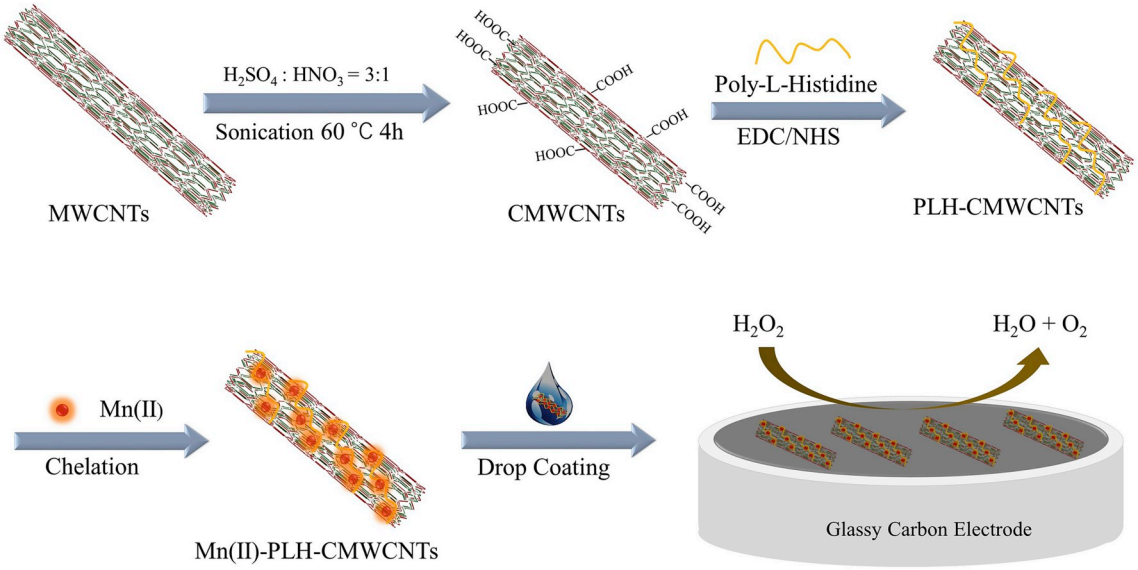

Scheme 1. Illustration in the preparation of Mn(II)-PLH-CMWCNT/GCE.

I_G ratio of PLH-CMWCNTs increased from 1.04 (CMWCNTs) to 1.17, which was attributed to the substitutional heteroatoms of imidazole groups on the PLH side chain. The I_D/I_G value of Mn(II)-PLH-CMWCNT composite decreased to 1.06, suggesting the complexation of Mn(II) with PLH-CMWCNTs.

Further, FTIR spectroscopy was applied to characterize the structural and combinational properties of the Mn(II)-PLH-CMWCNT nanocomposite. As shown in Fig. 1B, the modification of PLH was clearly indicated by the increased intensity of C=C (1623 cm^{-1}), C=N (1608 cm^{-1}) and O-H stretching of carboxylic acid (1000 cm^{-1}) (curve c), which was attributed to the introduction of PLH [30,31]. Particularly, PLH formed amide bonds with CMWCNT by amidation reaction, due to the N-H in-plane bending and the N-C stretching vibration of the -CO-NH- group, a significant peak of the amide band was observed at 1541 cm^{-1} [32,33]. The complexation of Mn(II) decreased the intensity of the above stretching peaks to some extent (curve d).

Transmission Electron Microscope (TEM) and Energy-dispersive X-ray spectroscopy (EDXS) were employed to characterize the microstructures of the Mn(II)-PLH-CMWCNT nanocomposite. Raw MWCNTs with irregular hollow tubular structures could be seen clearly in Fig. 2A. A coil-like structure of MWCNTs appeared in Fig. 2B, and an agglomerated structure was observed with the composite system due to the immobilized metal complex [25]. The inset shows a typical single CMWCNT with defect and its open terminal. A high-resolution micrograph of the PLH modified CMWCNTs is shown in Fig. 2C, which intuitively confirmed the modification of a ~3 nm thick PLH layer. Energy-dispersive X-ray spectrometry (EDXS) of the Mn(II)-PLH-CMWCNT nanocomposite is displayed in Fig. 2D, the peak of N was from the PLH, the Mn peaks was attributed to the complexation of Mn(II), while the Cu peaks resulted from the copper grid. When CMWCNT was directly mixed with Mn(II) to form Mn(II)-CMWCNT composite, Mn(II) could not be able to bind tightly to CMWCNT without PLH, and would be redissolved in the supernatant after washing and centrifugation, thus the EDXS of the prepared composite had no Mn (supplementary material S1), which confirmed the chelation of manganese ions with PLH. In summary, the Mn(II)-PLH-CMWCNT nanocomposite was successfully synthesized.

3.2. Electrochemical performance of the Mn(II)-PLH-CMWCNT/GCE

The charge transfer properties and the electroactive surface areas of the fabricated electrodes were investigated by CV in ferricyanide system, and the results are shown in Fig. 3 [34]. All the fabricated electrodes presented a couple of well-defined redox peaks of $[Fe(CN)_6]^{4-/3-}$. The effective surface area of an electrode can be estimated using the Randles–Sevcik equation (6) [35]:

$$i_p = 2.69 \times 10^5 n^{3/2} D^{1/5} C_0 v^{1/2} A_{eff} \quad (6)$$

where i_p is the redox peak current (μA); n represents the number of electrons transferred in the redox reaction; D relates to the diffusion coefficient of the molecules in solution; C_0 is the concentration of the probe molecule which is 10 mM; v is the scan rate (50 mV s^{-1}); A_{eff} denotes the effective surface area of the electrode (cm^2). It was found that the Mn(II)-PLH-CMWCNT/GCE (curve d) had an effective surface area of 0.13 cm^2, which was 1.75, 1.50 and 1.24 times higher than that of the bare GCE (curve a), CMWCNT/GCE (curve b) and PLH-CMWCNT/GCE (curve c). Comparing with bare GCE, the ratio of A_{eff} of CMWCNT/GCE was 1.17, while the ratio of A_{eff} of PLH-CMWCNT/GCE was 1.42. This may aid in enhancing the charge transfer reaction at PLH functionalized CMWCNTs, which will in turn facilitate high detection sensitivity at the fabricated biosensor. When there is no $[Fe(CN)_6]^{4-/3-}$ in the solution, the redox process cannot be achieved due to the lack of redox species and the four modified electrodes had almost no redox peaks (supplementary material S2).

3.3. Electrocatalytic activity of Mn(II)-PLH-CMWCNT/GCE to H_2O_2

Electrocatalytic activity of the fabricated electrodes was investigated by CV in 0.1 M sodium bicarbonate solution. In the solution without H_2O_2, the Mn-complex modified electrode has almost no response (supplementary material S3), but exhibits a good electrical signal response in the presence of H_2O_2. As shown in Fig. 4, at the bare GCE (curve a), the oxidation peak of H_2O_2 was quite small, indicating a weak disproportionation of H_2O_2 on the surface of bare GCE. Due to the enlarged effective surface area and the π-π stacking interaction between imidazole groups of PLH and CMWCNTs, the disproportionation of H_2O_2 was enhanced to a certain extent at the CMWCNT/GCE (curve b) and PLH-CMWCNT/GCE (curve c). However, with the complexation of Mn(II) (curve d), a sharp oxidation peak was found around 300 mV, which was chosen as the operating voltage in the following experiments. A similar phenomenon was observed by CA technique (Fig. 4B). This is because under *in-vitro* conditions, hydrogen peroxide and superoxide anion were found to be unstable in the presence of Mn(II), and Mn(II) catalyzes the disproportionation of H_2O_2 in the presence of [36].

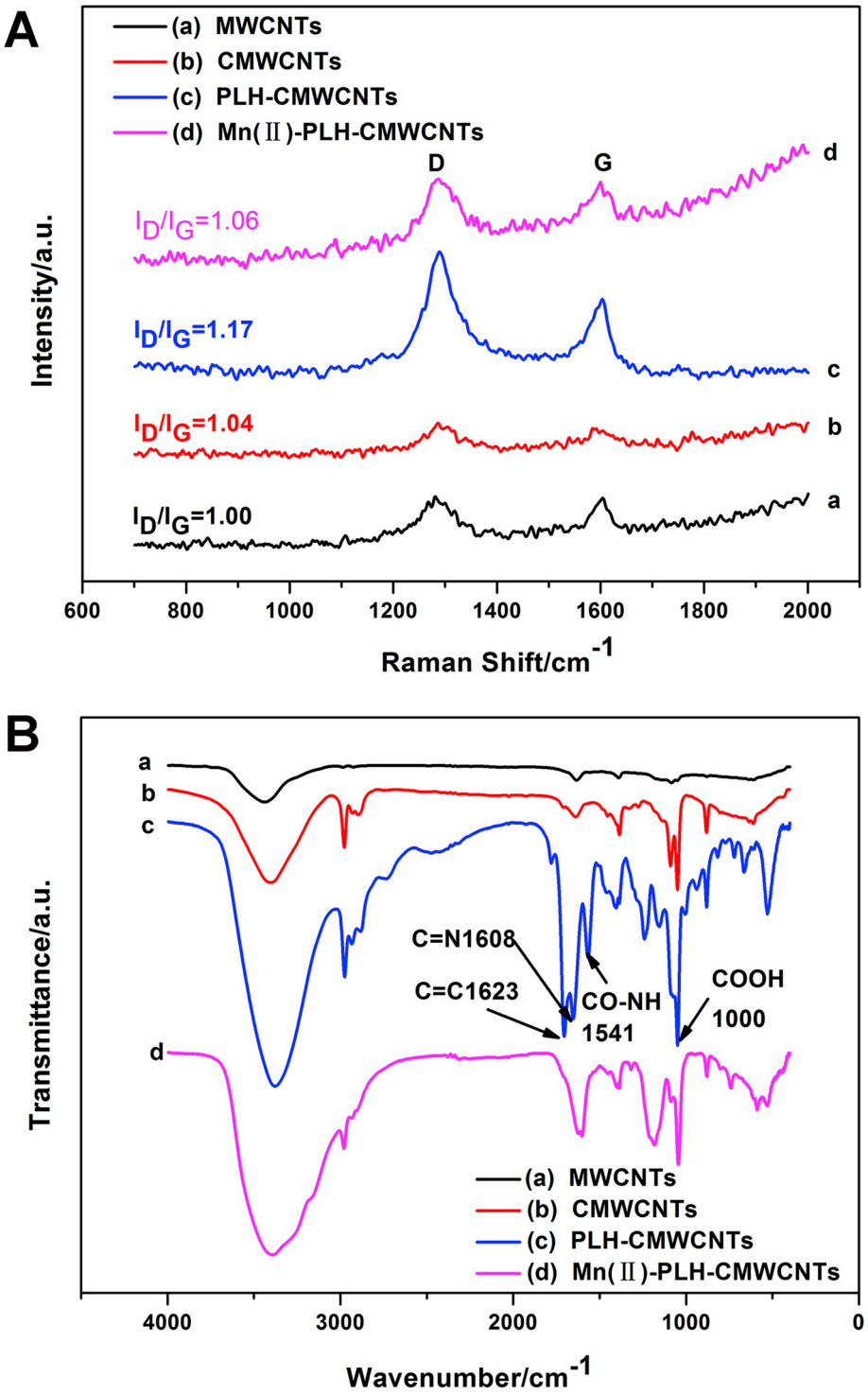

Fig. 1. Raman spectra (A) and FTIR spectra (B) of MWCNTs (curve a), CMWCNTs (curve b), PLH-CMWCNTs (curve c), and Mn(II)- PLH-CMWCNTs (curve d).

The mechanism of this catalase-like activity could be elaborated by the following reactions:

$$H_2O_2 + Mn(II) \rightarrow OH\cdot + OH^- + Mn(III) \quad (1)$$

$$OH\cdot + HCO_3^- \rightarrow H_2O + CO_3^-\cdot \quad (2)$$

$$CO_3^-\cdot + H_2O_2 \rightarrow HCO_3^- + O_2^-\cdot + H^+ \quad (3)$$

$$O_2^-\cdot + Mn(III) \rightarrow Mn(II) + O_2 \quad (4)$$

$$(sum)\cdot 2H_2O_2 \rightarrow 2H_2O + O_2 \quad (5)$$

When Mn(II) is complexed with ligand, it is readily oxidized by H_2O_2 to Mn(III) (reaction 1). The participation of , causing a decrease in the redox potential of the Mn(III) ⇆ Mn(II) couple (reaction 1 and 4), permits facile reaction of H_2O_2 to generate hydroxyl radical (OH·) and superoxide anion ($O_2^-\cdot$) (reaction 1, 2 and 3). It is believed that the $CO_3^-\cdot$ radical generated by reactions with OH· would be more effective in promoting H_2O_2 decomposition than OH· alone (reaction 2, 3 and 5). In any case, direct determination of the redox potential of Mn(II)-complexes may help to explain the unique requirement for in the decomposition of H_2O_2 [37–41]. These reaction mechanisms are consistent

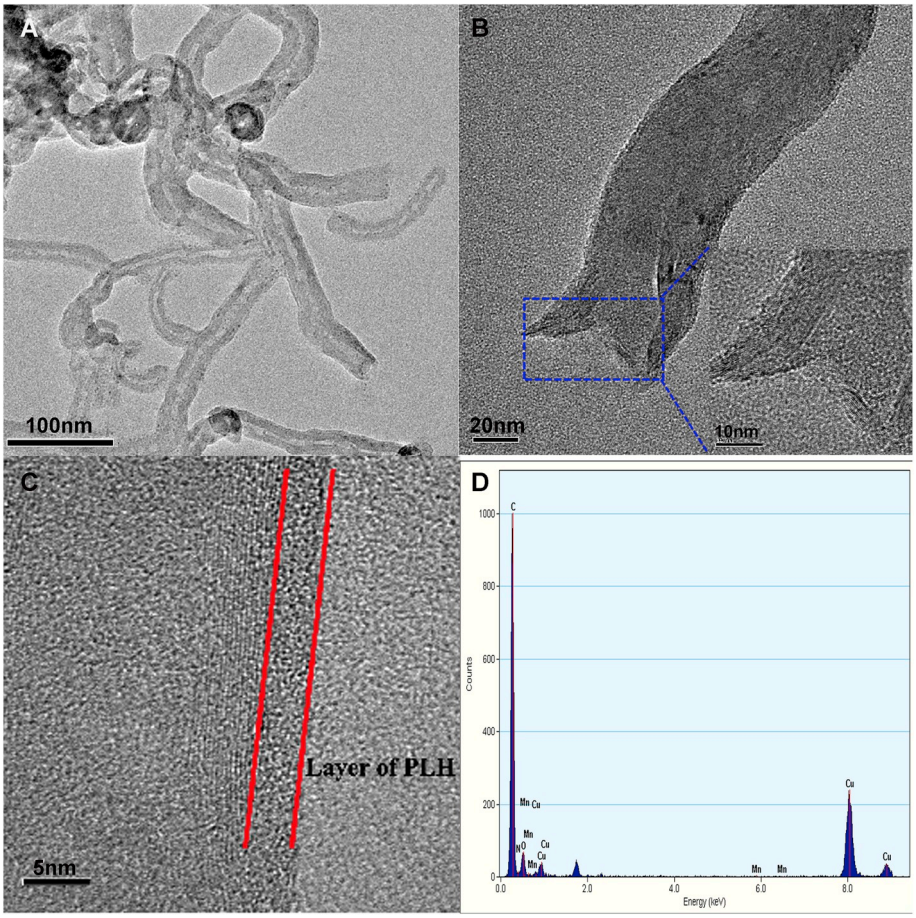

Fig. 2. Transmission electron micrographs of MWCNTs (A), CMWCNTs (B) (insert shows the carboxylated open end), PLH-CMWCNTs (C), and EDXS spectrum of Mn (II)-PLH-CMWCNTs (D).

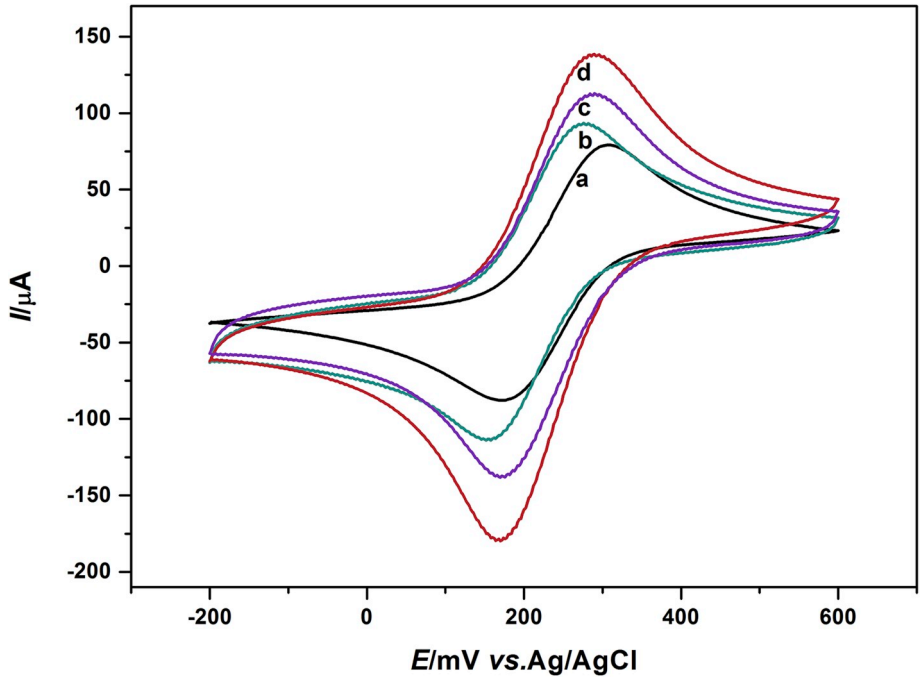

Fig. 3. Cyclic voltammograms of 10 mM $[Fe(CN)_6]^{4-/3-}$ at a bare GCE (curve a), a CMWCNT/GCE (curve b), a PLH-CMWCNT/GCE (curve c) and a Mn(II)-PLH-CMWCNT/GCE (curve d) recorded in 0.1 M KCl. Scan rate: 50 mV s^{-1}.

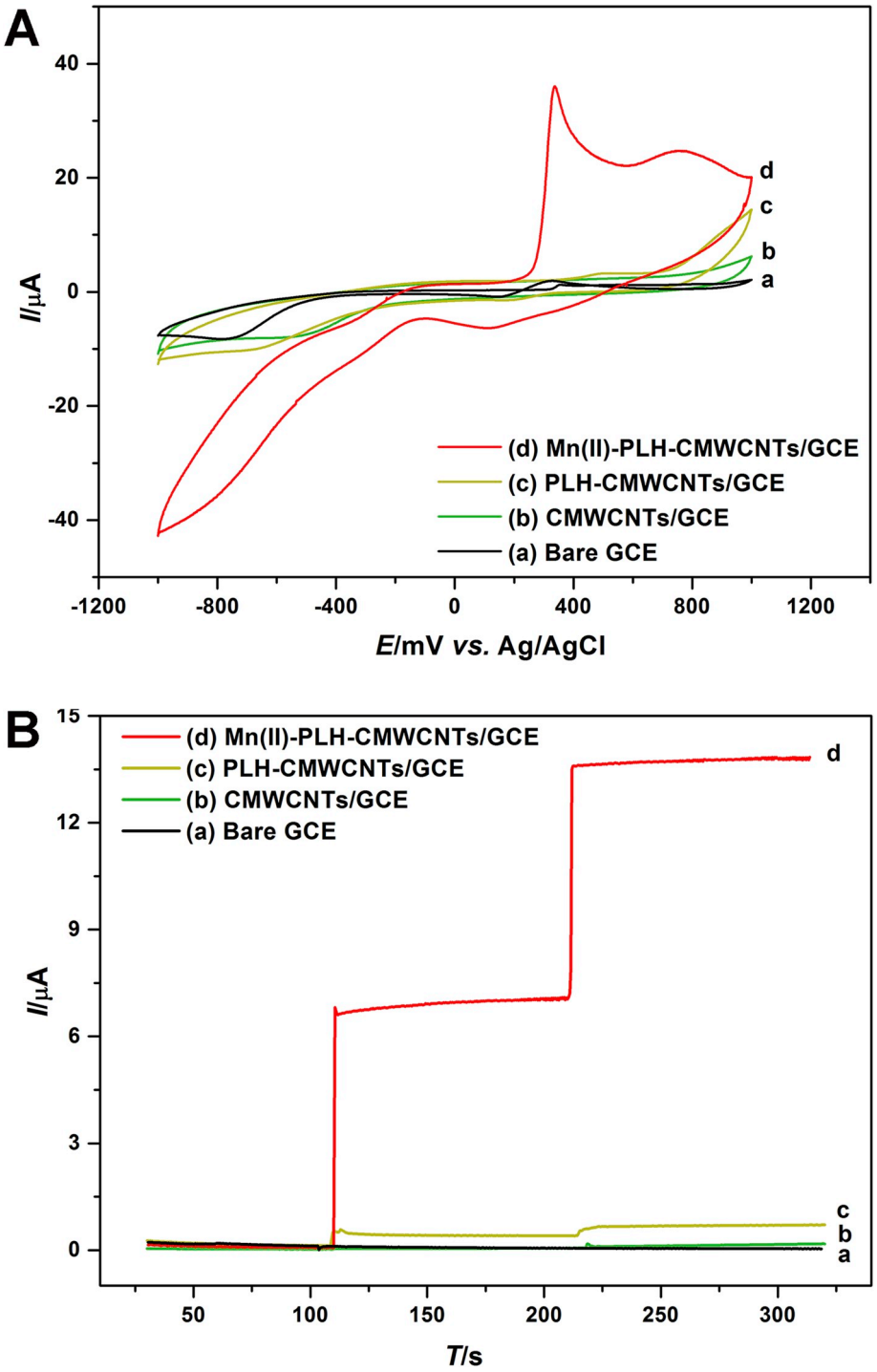

Fig. 4. Cyclic voltammograms (A) and chronoammograms (B) of the bare GCE (curve a), CMWCNT/GCE (curve b), PLH-CMWCNT/GCE (curve c) and Mn(II)-PLH-CMWCNT/GCE (curve d) toward H_2O_2 in 0.1 M $NaHCO_3$ solution. Scan rate: 50 mV s^{-1}, H_2O_2 concentration: 0.2 mM (A); operating voltage: 300 mV, H_2O_2 concentration: 0.2, 0.4 mM (B).

with previous research results. Lessa et al. reported reactivity studies of a mononuclear water-soluble complex, Mn(II)(HPClNOL)(η_1-NO_3)(η_2-NO_3), where HPClNOL = 1-(bis-pyridin-2-ylmethyl-amino)-3-chloropropan-2-ol, toward peroxides (H_2O_2 and tert-butyl hydroperoxide). The results supported the hypothesis that the main pathway for catalyst inactivation was via protonation, by monitoring the peroxidase (in CH_3CN) and catalase (in aqueous solution) activities of the complex [42]. Maneiro et al. prepared a new type of manganese-Schiff base complex based on N, N′-bis(salicylidene)-1,2-diimino-2-methylethane as peroxidase mimics, and found that the rate of peroxidase activity of the present complexes was significantly higher than that of other series of Mn-Schiff base compounds, probably due to their versatility in adopting in solution a structure that allowed the coordination of the H_2O_2 substrate molecule to the manganese [43]. Here, after complexation with manganese ions, the Mn(II)-PLH-CMWCNT/GCE exhibited a dramatically higher electrocatalytic activity toward H_2O_2, indicating that the fabricated biosensor could be applied for the determination of H_2O_2.

Moreover, the effect of scan rate at the Mn(II)-PLH-CMWCNT/GCE was investigated by cyclic voltammetry and the results are shown in

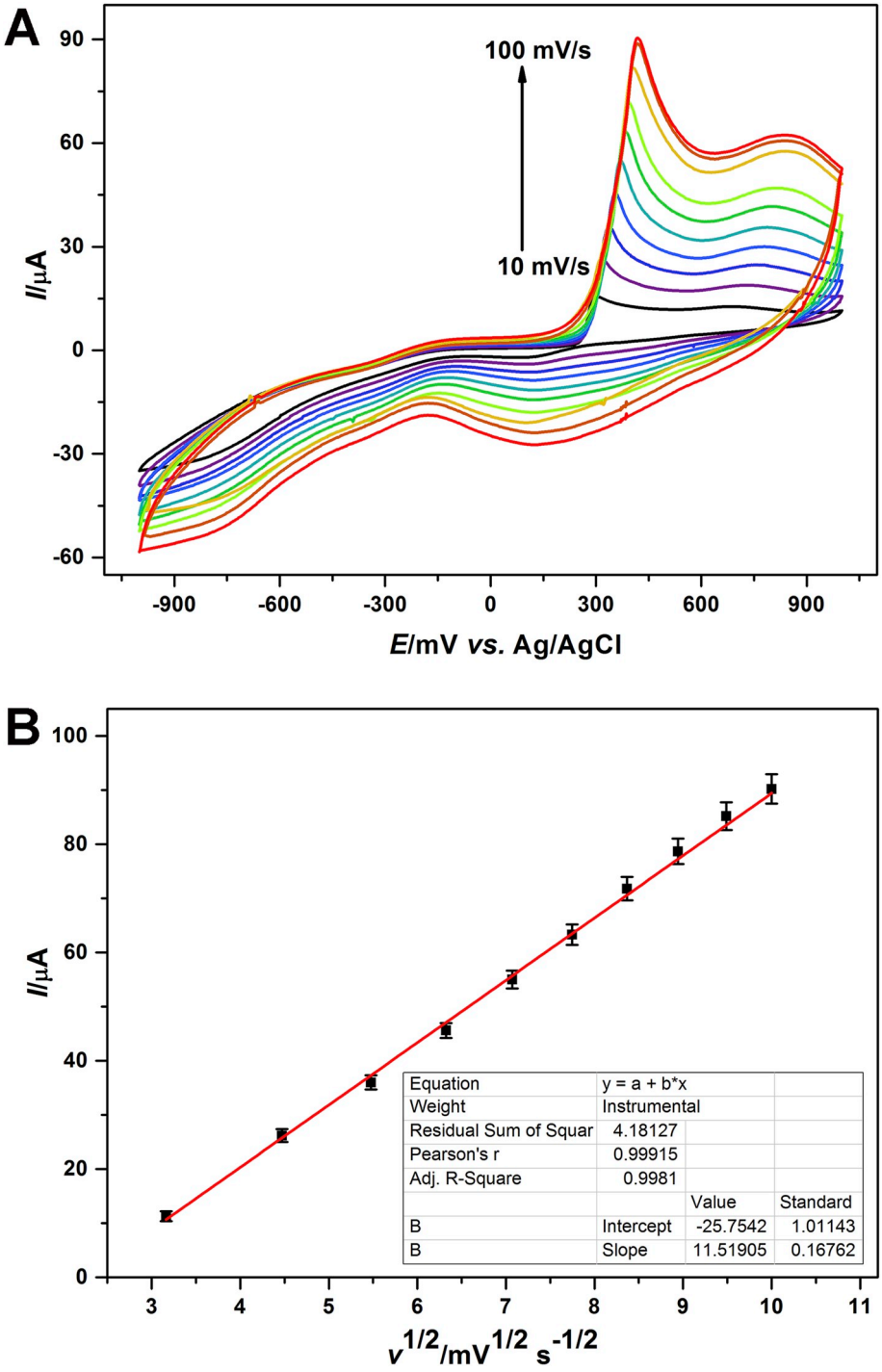

Fig. 5. (A) Cyclic voltammograms of the Mn(II)-PLH-CMWCNT/GCE toward 0.2 mM H_2O_2 in 0.1 M $NaHCO_3$ solution with different scan rate (10, 20, 30, 40, 50, 60, 70, 80, 90, 100 mV s^{-1}). (B) Linear relationship of the oxidation peak currents (I_p) versus the square root of scan rate ($v^{1/2}$). Error bars = ± standard deviation, n = 5.

Fig. 5A. The H_2O_2 oxidation current was observed to increase with scan rate between 10.0 and 100.0 mV s^{-1}. A linear relationship was fitted between the oxidation peak currents and the square root of scan rate ($v^{1/2}$) (as shown in Fig. 5B). The linear regression equation was expressed as $I_p = 11.52v^{1/2}$-25.75 (v in mV s^{-1}, $R^2 = 0.998$), which suggested a diffusion-controlled electrochemical process. The diffusion coefficient of H_2O_2 could be calculated according to equation (6) [44]. Based on Equation (6), the slope of a linear I_p versus $\nu^{½}$ plot was used to estimate D_o to be 1.35×10^{-6} cm^2 s^{-1}, which is in agreement with the reported vaule (1.62×10^{-6} cm^2 s^{-1}) [45].

3.4. Effect of sodium bicarbonate concentration

For the manganese-dependent H_2O_2 disproportionation in Mn/ system, the catalase-like activity of Mn is greatly augmented by the presence of amino acids and is extremely sensitive to small changes in concentration [37,46–50]. In this study, Mn was solidly immobilized in the Mn(II)-PLH-CMWCNT nanocomposite on electrode surface, and the content was determined. Thus, the electrocatalytic activity of the modified electrode was largely dependent on concentration. Therefore, the effect of sodium bicarbonate concentration on the electrochemical

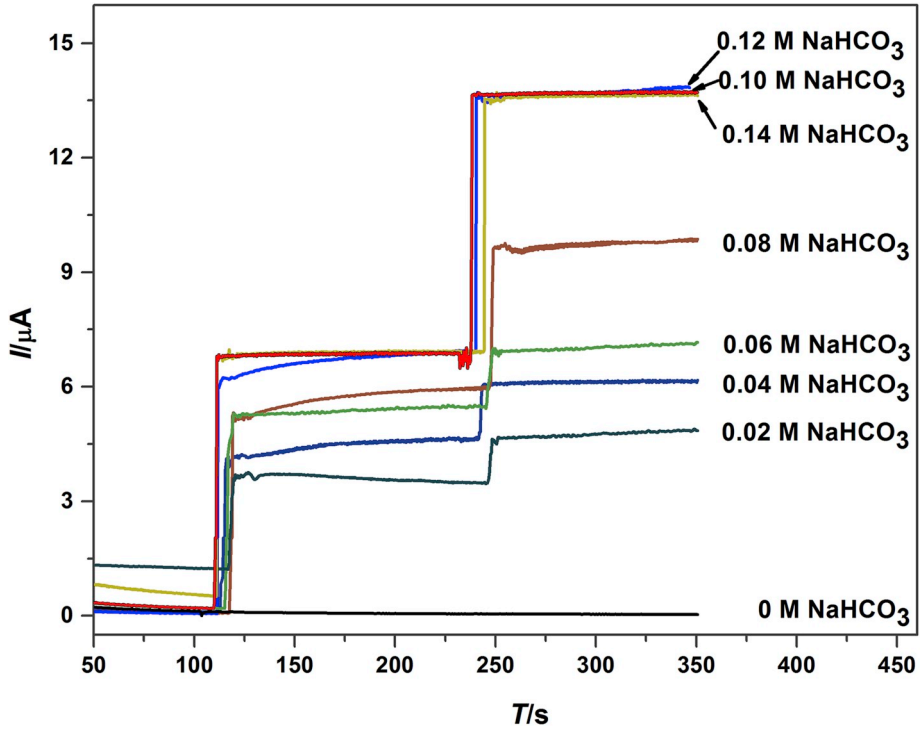

Fig. 6. Chronoammograms of Mn(II)-PLH-CMWCNT/GCE toward 0.2, 0.4 mM H_2O_2 in 0–0.14 M $NaHCO_3$ solutions (Operating voltage: 300 mV).

responses toward 0.2, 0.4 mM H_2O_2 at Mn(II)-PLH-CMWCNT/GCE was studied by CA technique in the range of 0–0.14 M $NaHCO_3$ solutions. As shown in Fig. 6, along with the increase of sodium bicarbonate concentration, the response currents increased and reached the maximum at 0.1 M $NaHCO_3$ then remained stable thereafter. Thus, 0.1 M $NaHCO_3$ was chosen as the working solution.

3.5. Electrochemical determination of H_2O_2

Under the chosen conditions (0.1 M $NaHCO_3$, 300 mV), CA technique was applied for the quantitative determination of H_2O_2, and the results were shown in Fig. 7. As can be seen in Fig. 7A, the amperometric response current increased with H_2O_2 concentration from 0.002 mM to 4.0 mM. Then, the response current growth rate decreased and reached the peak. The fabricated biosensor was also demonstrated to reach 95% of the steady state current within 3 s. After 5 independent repetitive experiments, a calibration curve was fitted, as shown in Fig. 7B. The response currents presented a linear relationship toward H_2O_2 concentration over the range of 0.002–1.0 mM. According to the slope of the calibration plot, the sensitivity of the prepared biosensor was calculated to be 464.18 μA mM^{-1} cm^{-2} (32.81 μA mM^{-1}), and the limit of detection (LOD) was estimated to be 0.5 μM based on a signal-to-noise ratio of 3.

This phenomenon conformed to a classical enzymatic kinetics. In the reaction kinetic analysis of a biosensor, the Eadie-Hofstee form of the Michaelis–Menten equation is an efficient method. For amperometric biosensors, the Eadie-Hofstee form could be expressed as [51]:

$$\frac{1}{I_{SS}} = \frac{1}{I_{max}} + \frac{K_m^{app}}{I_{max}}\frac{1}{C} \quad (7)$$

where I_{SS} is the steady-state current, C is the bulk concentration of the substrate, I_{max} is the maximum current measured under saturated substrate conditions, and K_m^{app} is the apparent Michaelis-Menten constant, a characteristic parameter of the enzyme-substrate kinetics. Fig. 8 shows an Eadie-Hofstee plot of the reciprocal of the steady-state current versus reciprocal of H_2O_2 concentration. From the slope and intercept of the plot, the K_m^{app} of the fabricated H_2O_2 biosensor was estimated to be 0.50 mM. This value is lower than most of the reported enzymatic H_2O_2 biosensors (as shown in Table 1), indicating that the synthesized Mn(II)-PLH-CMWCNT nanocomposite had excellent catalase-like activity.

Analytical parameters of the current enzyme-mimicking H_2O_2 biosensor were compared with the enzymatic H_2O_2 biosensors previously reported by others (Table 1). Considering the LOD, linear range, sensitivity and K_m^{app}, the proposed Mn(II)-PLH-CMWCNT/GCE exhibited better performance. This might because that the Mn(II)-PLH redox-active unit expressed ultrasensitive catalase-like activity as the catalytic active center. Meanwhile, the PLH-CMWCNTs enhanced electrocatalytic active area promoting a large amount of H_2O_2 to be adsorbed onto the electrode surface, and supplied a necessary pathway for electron transfer from substrate to electrode directly.

3.6. Stability, reproducibility, selectivity and applicability of the prepared H_2O_2 biosensor

For the evaluation of a biosensor, the long-term stability, reproducibility, selectivity and applicability are necessary parameters. The long-term stability of the fabricated biosensor was investigated by examining the response currents toward 0.2 mM H_2O_2 for an interval of 15 days. When not in use, the electrodes were kept at room temperature. The response currents could remain 92.3% after 90 days (Fig. 9A), indicating a good stability. Using the same procedures, five electrodes were fabricated and inspected the amperometric responses toward 0.2, 0.4 mM H_2O_2 (Fig. 9B). The relative standard deviation (RSD) of sensitivities was calculated to be 4.15%, which denoted a good reproducibility. In practice, some electrochemically active substances such as glucose (Glu), uric acid (UA), acetaminophen (AP), dopamine (DA), ascorbic acid (AA), might interfere the detection of H_2O_2. Selectivity or anti-interference capability of the present biosensor was assessed by comparing the amperometric responses of H_2O_2 and the interferences. As can be seen in Fig. 9C, at the level of physical concentration, Glu and UA had almost no response, although AP, DA, and AA had certain responses, which could be neglected comparing with the high sensitivity toward H_2O_2, indicating the high selectivity of the present H_2O_2

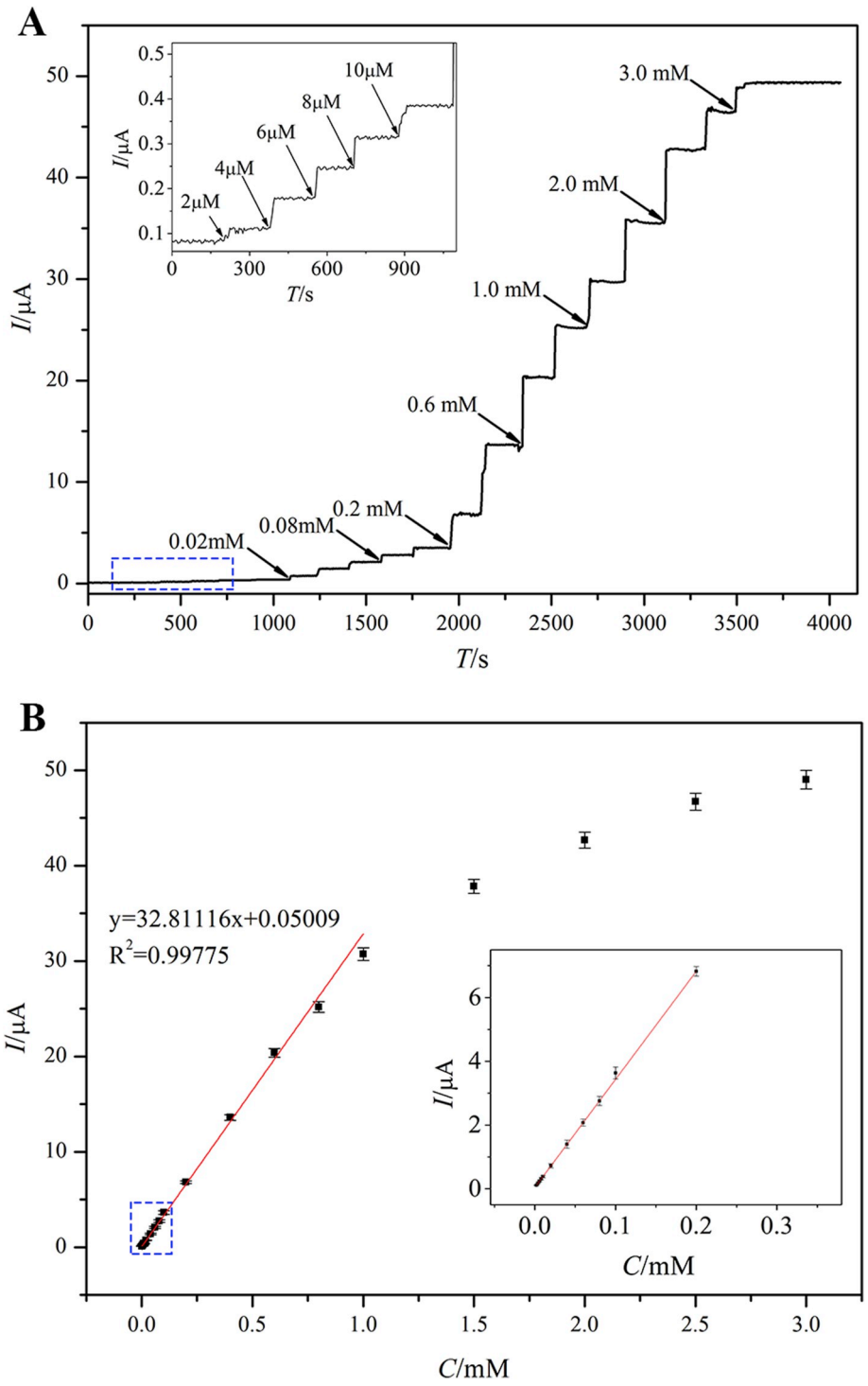

Fig. 7. (A) Amperometric responses of Mn(II)-PLH-CMWCNT/GCE at the operating voltage of 300 mV in 0.1 M $NaHCO_3$ solution toward successive additions of H_2O_2; (B) Calibration curve of the amperometric responses. Inset shows the regions of lower concentrations. Error bars = ± standard deviation, n = 5.

biosensor.

The above excellent analytical characteristics permitted the applicability of the biosensor in practical determination. The applicability of the prepared biosensor was testified by detecting H_2O_2 in diluted disinfectant and disinfected fetal bovine serum (FBS) samples. FBS was diluted to 1% with 0.1 M $NaHCO_3$ solution, centrifuged in 12000 rpm for 20 min, then filtrated by three 0.2 μm sterilizing grade membrane filters in series. All samples obtained were spiked with H_2O_2 standard solutions. As shown in Table 2, the recovery was found in the range of 96–105%, and the RSD ranged from 2.87% to 4.03%.

4. Conclusions

In summary, an efficient catalase-mimicking nanocomposite of Mn (II)-poly-L-histidine-carboxylated multi walled carbon nanotubes was successfully synthesized and applied to H_2O_2 sensing. Serving as the catalytic active center, Mn(II)-PLH redox-active unit presented ultrasensitive catalase-like activity, which could catalyze the disproportionation of H_2O_2 efficiently in the presence of . Meanwhile, PLH-CMWCNTs enlarged the electrode effective surface area, promoting a large amount of H_2O_2 to adsorb on the sensing interface.

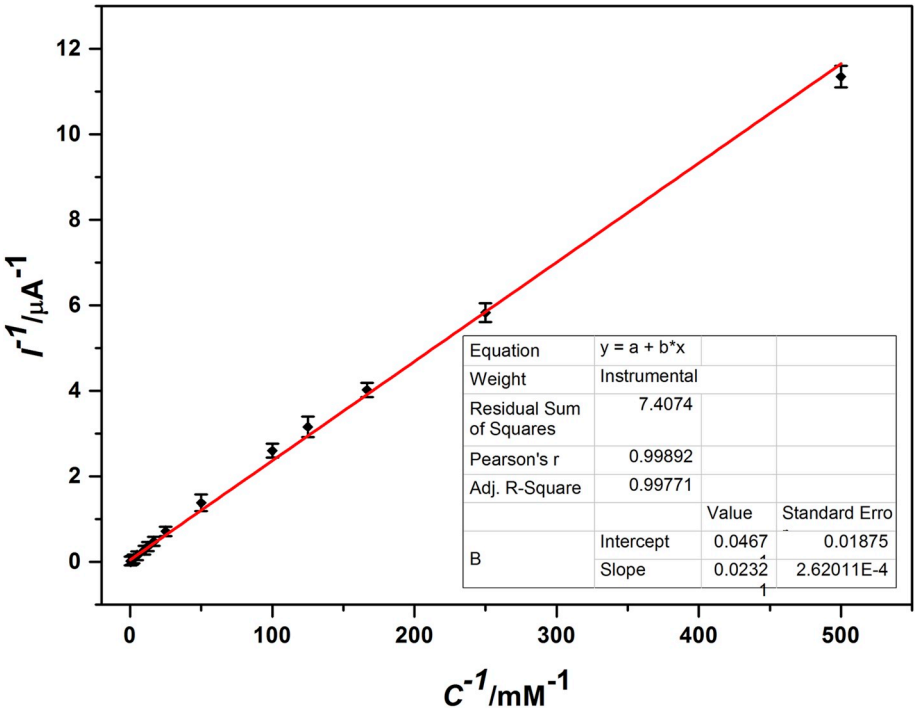

Fig. 8. Eadie-Hofstee plot of the prepared biosensor. Error bars = ± standard deviation, n = 5.

Table 1
Comparison of analytical parameters between the prepared hydrogen peroxide biosensor and previously reported enzymatic sensors.

Interface modification	LOD (μM)	Liner range (mM)	Sensitivity(μA mM^{-1} cm^{-2})	K_m^{app} (mM)	Reference
HRP [a]-nano-Au/PAMAM [b] dendrimer/cystamine/AuE [c]	2	0.01–2.5	530	0.52	[54]
HRP-Nafion-Sonogel-Carbon Electrode	1.6	0.004–0.1	12.8	0.295	[55]
MWCNTs [d]/MG [e]/HRP/GCE [f]	0.5	0.0005–0.02	—	1.8	[56]
HRP/Poly(GMA [g]-co-VFc [h])/GCE	2.6	2.0–30	10.42×10^{-3}	1.14	[57]
Mn(II)-PLH-CMWCNT/GCE	0.5	0.002–1.0	464.18	0.50	This work

[a] Horseradish peroxidase.
[b] Poly(amidoamine).
[c] Gold electrode.
[d] Multiwalled carbon nanotubes.
[e] Methylene green.
[f] Glassy carbon electrode.
[g] Glycidyl methacrylate.
[h] Vinylferrocene.

Precisely based on the above mechanisms, the fabricated non-enzymatic H_2O_2 biosensor expressed excellent performances with higher sensitivity, broader liner range, lower LOD and K_m^{app}, than most of the reported enzymatic H_2O_2 sensors. Furthermore, the current biosensor was applied to detection of H_2O_2 in real-life samples. This work provided a promising strategy for development of novel nanomaterials in electrocatalysis, biosensing and relevant fields.

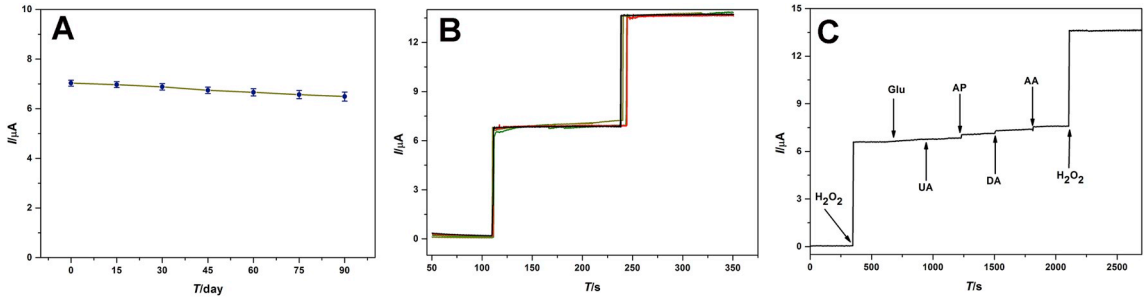

Fig. 9. (A) Response currents of the same Mn(II)-PLH-CMWCNT/GCE toward 0.2 mM H_2O_2 with a 15-day interval. Error bars = ± standard deviation, n = 5. (B) Amperometric responses of five electrodes toward 0.2 mM H_2O_2. (C) Interference test of the fabricated biosensor in 0.2 mM H_2O_2 and other interfering substances (5.0 mM Glu, 0.2 mM UA, 0.2 mM AP, 0.2 mM DA and 0.2 mM AA).

Table 2
Determination of H_2O_2 in real-life samples by the prepared biosensor.

Sample	HPLC detected (mM)	This method detected (mM)	H_2O_2 added (mM)	H_2O_2 found (mM)	Recovery (%)	RSD (%, n = 5)
Disinfectant 1 [a]	0.216	0.194	0.1	0.299	105.00	4.03
Disinfectant 2 [a]	0.189	0.216	0.2	0.409	96.50	3.97
Disinfectant 3 [a]	0.221	0.208	0.3	0.515	102.33	2.95
FBS sample 1	—	—	0.1	0.096	96.00	3.64
FBS sample 2	—	—	0.2	0.207	103.50	2.87
FBS sample 3	—	—	0.3	0.293	97.67	3.86

[a] 5×10^3 times diluted with 0.1 M $NaHCO_3$, and the H_2O_2 concentration of the original liquid is about 1 M.

Conflicts of interest

The authors declare no conflict of interest.

Acknowledgements

The financial supports from the National Natural Science Foundation of China (Grant Nos. 81671779 and 81871451), the Doctoral Starting up Foundation of Hebei University of Science and Technology, China (81/1181296) and the Key Projects of Tianjin Science and Technology Support Program (No. 16YFZCSY00440) are acknowledged.

Appendix A. Supplementary data

Supplementary data to this article can be found online at https://doi.org/10.1016/j.ab.2018.12.007.

References

[1] E.A. Veal, A.M. Day, B.A. Morgan, Hydrogen peroxide sensing and signaling, Mol. Cell 26 (2007) 1–14.
[2] E. Veal, A. Day, Hydrogen peroxide as a signaling molecule, Antioxidants Redox Signal. 15 (2011) 147–151.
[3] W. Chen, S. Cai, Q.-Q. Ren, W. Wen, Y.-D. Zhao, Recent advances in electrochemical sensing for hydrogen peroxide: a review, Analyst 137 (2012) 49–58.
[4] J.M. Sobota, J.A. Imlay, Iron enzyme ribulose-5-phosphate 3-epimerase in Escherichia coli is rapidly damaged by hydrogen peroxide but can be protected by manganese, Proc. Natl. Acad. Sci. Unit. States Am. 108 (2011) 5402–5407.
[5] P. Gimeno, C. Bousquet, N. Lassu, A.-F. Maggio, C. Civade, C. Brenier, L. Lempereur, High-performance liquid chromatography method for the determination of hydrogen peroxide present or released in teeth bleaching kits and hair cosmetic products, J. Pharmaceut. Biomed. Anal. 107 (2015) 386–393.
[6] R. Zhang, W. Chen, Recent advances in graphene-based nanomaterials for fabricating electrochemical hydrogen peroxide sensors, Biosens. Bioelectron. 89 (1) (2017) 249–268.
[7] D. Yu, P. Wang, Y. Zhao, A. Fan, Iodophenol blue-enhanced luminol chemiluminescence and its application to hydrogen peroxide and glucose detection, Talanta 146 (2016) 655–661.
[8] F. Liu, T. Bing, D. Shangguan, M. Zhao, N. Shao, Ratiometric fluorescent biosensing of hydrogen peroxide and hydroxyl radical in living cells with lysozyme–silver nanoclusters: lysozyme as stabilizing ligand and fluorescence signal unit, Anal. Chem. 88 (2016) 10631–10638.
[9] D. Mukhopadhyay, P. Dasgupta, D.S. Roy, S. Palchoudhuri, I. Chatterjee, S. Ali, S.G. Dastidar, A sensitive in vitro spectrophotometric hydrogen peroxide scavenging assay using 1,10-phenanthroline, Free Radic. Antioxidants 6 (2016) 124–132.
[10] Q.-M. Jiang, M.-R. Zhang, L.-Q. Luo, G.-B. Pan, Electrosynthesis of bismuth nanodendrites/gallium nitride electrode for non-enzymatic hydrogen peroxide detection, Talanta 171 (2017) 250–254.
[11] C.M. Parnell, F. Watanabe, U.B. Nasini, B.C. Berry, T. Mitchell, A.U. Shaikh, A. Ghosh, Electrochemical sensing of hydrogen peroxide using a cobalt(III) complex supported on carbonaceous nanomaterials, J. Electroanal. Chem. 740 (2015) 37–44.
[12] S. Iijima, Helical microtubules of graphitic carbon, Nature 354 (1991) 56–58.
[13] N.G. Mphuthi, A.S. Adekunle, O.E. Fayemi, L.O. Olasunkanmi, E.E. Ebenso, Phthalocyanine doped metal oxide nanoparticles on multiwalled carbon nanotubes platform for the detection of dopamine, Sci. Rep. 7 (2017) 43181.
[14] S. Zhang, L. Kang, X. Wang, L. Tong, L. Yang, Z. Wang, K. Qi, S. Deng, Q. Li, X. Bai, F. Ding, J. Zhang, Arrays of horizontal carbon nanotubes of controlled chirality grown using designed catalysts, Nature 543 (2017) 234–238.
[15] J. Park, O.G. Reid, J.L. Blackburn, G. Rumbles, Photoinduced spontaneous free-Carrier generation in semiconducting single-walled carbon nanotubes, Nat. Commun. 6 (2015) 8809.
[16] Y. Mao, G. Li, Y. Guo, Z. Li, C. Liang, X. Peng, Z. Lin, Foldable interpenetrated metal-organic frameworks/carbon nanotubes thin film for lithium–sulfur batteries, Nat. Commun. 8 (2017) 14628.
[17] V. Datsyuk, M. Kalyva, K. Papagelis, J. Parthenios, D. Tasis, A. Siokou, I. Kallitsis, C. Galiotis, Chemical oxidation of multiwalled carbon nanotubes, Carbon 46 (2008) 833–840.
[18] G.A. DiLabio, E.R. Johnson, Lone Pair−π and π−π interactions play an important role in proton-coupled electron transfer reactions, J. Am. Chem. Soc. 129 (2007) 6199–6203.
[19] A. Takai, C.P. Gros, J.-M. Barbe, R. Guilard, S. Fukuzumi, Enhanced electron-transfer properties of cofacial porphyrin dimers through π–π interactions, Chem.-A Eur. J. 15 (2009) 3110–3122.
[20] I. Pecht, A. Levitzki, M. Anbar, The copper-poly-L-histidine complex. I. The environmental effect of the polyelectrolyte on the oxidase activity of copper ions, J. Am. Chem. Soc. 89 (1967) 1587–1591.
[21] Y. Hasebe, T. Akiyama, T. Yagisawa, S. Uchiyama, Enzyme-less amperometric biosensor for l-ascorbate using poly-l-histidine-copper complex as an alternative biocatalyst, Talanta 47 (1998) 1139–1147.
[22] J.R. Wispé, B.B. Warner, J.C. Clark, C.R. Dey, J. Neuman, S.W. Glasser, J.D. Crapo, L.Y. Chang, J.A. Whitsett, Human Mn-superoxide dismutase in pulmonary epithelial cells of transgenic mice confers protection from oxygen injury, J. Biol. Chem. 267 (1992) 23937–23941.
[23] A.K. Holley, S.K. Dhar, Y. Xu, D.K. St Clair, Manganese superoxide dismutase: beyond life and death, Amino Acids 42 (2012) 139–158.
[24] A. Anjem, S. Varghese, J.A. Imlay, Manganese import is a key element of the OxyR response to hydrogen peroxide in Escherichia coli, Mol. Microbiol. 72 (2009) 844–858.
[25] N. Saravanan, P. Mayuri, S.-T. Huang, A.S. Kumar, In-situ electrochemical immobilization of [Mn(bpy)2(H2O)2]2+ complex on MWCNT modified electrode and its electrocatalytic H2O2 oxidation and reduction reactions: a Mn-Pseudocatalase enzyme bio-mimicking electron-transfer functional model, J. Electroanal. Chem. 812 (2018) 10–21.
[26] Y. Chen, X.-M. Liu, X. Wu, X.-C. Liu, W.-H. Dong, B.-K. Han, X. Du, C. Zhang, Y.-Y. Zhang, H.-T. Wang, Q. Chen, An array of poly-l-histidine functionalized multi-walled carbon nanotubes on 4-aminothiophenol self-assembled monolayer and the application for sensitively glucose sensing, Electrochim. Acta 258 (2017) 988–997.
[27] Q. Zhao, H.D. Wagner, Raman spectroscopy of carbon–nanotube–based composites, Philos. Trans. R. Soc. London, Ser. A: Math. Phys. Eng. Sci. 362 (2004) 2407–2424.
[28] R.A. MacDonald, B.F. Laurenzi, G. Viswanathan, P.M. Ajayan, J.P. Stegemann, Collagen–carbon nanotube composite materials as scaffolds in tissue engineering, J. Biomed. Mater. Res. 74A (2005) 489–496.
[29] J. Gao, S. Zhang, M. Liu, Y. Tai, X. Song, Y. Qian, H. Song, Synergistic combination of cyclodextrin edge-functionalized graphene and multiwall carbon nanotubes as conductive bridges toward enhanced sensing response of supramolecular recognition, Electrochim. Acta 187 (2016) 364–374.
[30] J. Madhavan, S. Aruna, P.C. Thomas, M. Vimalan, S.A. Rajasekar, P. Sagayaraj, Growth and characterization of L-histidine hydrochloride monohydrate single crystals, Cryst. Res. Technol. 42 (2007) 59–64.
[31] T.A. Saleh, V.K. Gupta, Functionalization of tungsten oxide into MWCNT and its application for sunlight-induced degradation of rhodamine B, J. Colloid Interface Sci. 362 (2011) 337–344.
[32] C.Y. Tang, Y.-N. Kwon, J.O. Leckie, Effect of membrane chemistry and coating layer on physiochemical properties of thin film composite polyamide RO and NF membranes: I. FTIR and XPS characterization of polyamide and coating layer chemistry, Desalination 242 (2009) 149–167.
[33] Y.-N. Kwon, J.O. Leckie, Hypochlorite degradation of crosslinked polyamide membranes: II. Changes in hydrogen bonding behavior and performance, J. Membr. Sci. 282 (2006) 456–464.
[34] Y. Fang, D. Zhang, Y. Guo, Y. Guo, Q. Chen, Simple one-pot preparation of chitosan-reduced graphene oxide-Au nanoparticles hybrids for glucose sensing, Sensor. Actuator. B Chem. 221 (2015) 265–272.
[35] M. Ramanathan, M. Patil, R. Epur, Y. Yun, V. Shanov, M. Schulz, W.R. Heineman, M.K. Datta, P.N. Kumta, Gold-coated carbon nanotube electrode arrays: immunosensors for impedimetric detection of bone biomarkers, Biosens. Bioelectron. 77 (2016) 580–588.
[36] J. Varani, I. Ginsburg, D.F. Gibbs, P.S. Mukhopadhyay, C. Sulavik, K.J. Johnson, J.M. Weinberg, U.S. Ryan, P.A. Ward, Hydrogen peroxide-induced cell and tissue injury: protective effects of Mn2+, Inflammation 15 (1991) 291–301.
[37] E.R. Stadtman, B.S. Berlett, P.B. Chock, Manganese-dependent disproportionation of hydrogen peroxide in bicarbonate buffer, Proc. Natl. Acad. Sci. Unit. States Am. 87 (1990) 384–388.
[38] E.K. Hodgson, I. Fridovich, The mechanism of the activity-dependent luminescence of xanthine oxidase, Arch. Biochem. Biophys. 172 (1976) 202–205.
[39] D. Behar, G. Czapski, I. Duchovny, Carbonate radical in flash photolysis and pulse radiolysis of aqueous carbonate solutions, J. Phys. Chem. 74 (1970) 2206–2210.
[40] M.B. Yim, B.S. Berlett, P.B. Chock, E.R. Stadtman, Manganese(II)-bicarbonate-mediated catalytic activity for hydrogen peroxide dismutation and amino acid oxidation: detection of free radical intermediates, Proc. Natl. Acad. Sci. U. S. A. 87 (1990) 394–398.
[41] S.I. Liochev, I. Fridovich, Carbon dioxide mediates Mn(II)-catalyzed decomposition of hydrogen peroxide and peroxidation reactions, Proc. Natl. Acad. Sci. U. S. A. 101 (2004) 12485–12490.
[42] J.A. Lessa, A. Horn, É.S. Bull, M.R. Rocha, M. Benassi, R.R. Catharino, M.N. Eberlin, A. Casellato, C.J. Noble, G.R. Hanson, G. Schenk, G.C. Silva, O.A.C. Antunes,

C. Fernandes, Catalase vs peroxidase activity of a manganese(II) compound: identification of a Mn(III) − (μ-O)2 − Mn(IV) reaction intermediate by electrospray ionization mass spectrometry and electron paramagnetic resonance spectroscopy, Inorg. Chem. 48 (2009) 4569–4579.

[43] M. Maneiro, M.R. Bermejo, M.I. Fernández, E. Gómez-Fórneas, A.M. González-Noya, A.M. Tyryshkin, A new type of manganese-Schiff base complex, catalysts for the disproportionation of hydrogen peroxide as peroxidase mimics, New J. Chem. 27 (2003) 727–733.

[44] X. Yan, Y. Gu, C. Li, L. Tang, B. Zheng, Y. Li, Z. Zhang, M. Yang, Synergetic catalysis based on the proline tailed metalloporphyrin with graphene sheet as efficient mimetic enzyme for ultrasensitive electrochemical detection of dopamine, Biosens. Bioelectron. 77 (2016) 1032–1038.

[45] T. Ravindran Madhura, P. Viswanathan, G. Gnana kumar, R. Ramaraj, Nanosheet-like manganese ferrite grown on reduced graphene oxide for non-enzymatic electrochemical sensing of hydrogen peroxide, J. Electroanal. Chem. 792 (2017) 15–22.

[46] K.G. Tikhonov, O.M. Zastrizhnaya, Y.N. Kozlov, V.V. Klimov, Composition and catalase-like activity of Mn(II)-bicarbonate complexes, Biochemistry (Mosc.) 71 (2006) 1270–1277.

[47] E.R. Stadtman, R.L. Levine, Free radical-mediated oxidation of free amino acids and amino acid residues in proteins, Amino Acids 25 (2003) 207–218.

[48] J. Dasgupta, A.M. Tyryshkin, Y.N. Kozlov, V.V. Klimov, G.C. Dismukes, Carbonate complexation of Mn2+ in the aqueous Phase: redox behavior and ligand binding modes by electrochemistry and EPR spectroscopy, J. Phys. Chem. B 110 (2006) 5099–5111.

[49] E.V. Bakhmutova-Albert, H. Yao, D.E. Denevan, D.E. Richardson, Kinetics and mechanism of peroxymonocarbonate formation, Inorg. Chem. 49 (2010) 11287–11296.

[50] Y.N. Kozlov, K.G. Tikhonov, O.M. Zastrizhnaya, V.V. Klimov, pH dependence of the composition and stability of MnIII–bicarbonate complexes and its implication for redox interaction of MnII with photosystemII, J. Photochem. Photobiol. B Biol. 101 (2010) 362–366.

[51] R.A. Kamin, G.S. Wilson, Rotating ring-disk enzyme electrode for biocatalysis kinetic studies and characterization of the immobilized enzyme layer, Anal. Chem. 52 (1980) 1198–1205.

[54] Z.M. Liu, Y. Yang, H. Wang, Y.L. Liu, G.L. Shen, R.Q. Yu, A hydrogen peroxide biosensor based on nano-Au/PAMAM dendrimer/cystamine modified gold electrode, Sensor. Actuator. B Chem. 106 (2005) 394–400.

[55] M. ElKaoutit, I. Naranjo-Rodriguez, M. Domínguez, M.P. Hernández-Artiga, D. Bellido-Milla, J.L. Hidalgo-Hidalgo de Cisneros, A third-generation hydrogen peroxide biosensor based on Horseradish Peroxidase (HRP) enzyme immobilized in a Nafion–Sonogel–Carbon composite, Electrochim. Acta 53 (2008) 7131–7137.

[56] A.K. Upadhyay, T.W. Ting, S.M. Chen, Amperometric biosensor for hydrogen peroxide based on coimmobilized horseradish peroxidase and methylene green in ormosils matrix with multiwalled carbon nanotubes, Talanta 79 (2009) 38–45.

[57] M. Şenel, E. Çevik, M.F. Abasıyanık, Amperometric hydrogen peroxide biosensor based on covalent immobilization of horseradish peroxidase on ferrocene containing polymeric mediator, Sensor. Actuator. B Chem. 145 (2010) 444–450.